# Numerical investigation on improving the heat storage and transfer performance of ceramic /D-mannitol composite phase change materials by bionic graded pores and nanoparticle additives

Daili Feng[a,b], Jianfu Nan[a], Yanhui Feng[a,b,*], Xinxin Zhang[a,b], Yuying Yan[c]

[a] School of Energy and Environmental Engineering, University of Science and Technology Beijing, Beijing 100083, China

[b] Beijing Key Laboratory of Energy Saving and Emission Reduction for Metallurgical Industry, University of Science and Technology Beijing, Beijing 100083, China

[c] Fluids & Thermal Engineering Research Group, Faculty of Engineering, University of Nottingham, Nottingham NG7 2RD, UK

(Tel: 62332599, *Corresponding authors. Email: yhfeng@me.ustb.edu.cn (Yanhui Feng))

## Abstract

To speed up the thermal response rate of the latent heat storage system, this research draws on the ideas of bionics and proposes two methods to enhance the performance of heat storage and heat transfer during phase change process. First, a biomimetic, double-gradient porous ceramic was applied to assemble phase change material (PCM) D-mannitol. The optimized gradient pore structure ensures that the composite possesses higher effective thermal conductivity, and better uniformity of phase interface evolution, with reasonable heat storage density. Numerical simulation predicts a 226 % increase in effective thermal conductivity comparing with the pure D-mannitol. Then, two kinds of carbon-based nanoparticles were added to further reinforce the heat transfer performance. Results found that graphite nanoparticles provide the most significant enhancement in the effective thermal conductivity of the composite material under the premise of ensuring a higher heat storage density. In conclusion, the effective thermal conductivity of the final composite achieves 3.33-fold increase due to the collaboration of the double gradient pore framework and the additive graphite nanoparticles. Accordingly, the overall heat transfer rate could be raised by 4.2 times, comparing with the pure PCM sample. This work demonstrates that the bidirectional gradient pore skeleton has significant advantages in heat storage and transfer over the single pore and unidirectional gradient pore.

**Key words:** double gradient pore framework, phase change materials, nanoparticles, thermal conductivity, numerical simulation

## 1. Introduction

Recent years have seen the gap between energy demand and supply continues to widen, with

supply failing to meet the increased demand. Given this, researchers are increasingly turning to exploring the recovery and utilization of heat energy. One of the main challenges of thermal energy storage (TES) is developing phase change materials (PCMs) [1] with the combination of high heat storage capacity, rapid charging/discharging, good reliability as well as high strength. As a commonly used PCM, sugar alcohol has a higher melting point that can be applied to a medium temperature (100~200 ℃) energy storage system, comparing with other organic PCMs. The latent heat of D-mannitol is twice that of paraffin wax, without segregation and corrosiveness. Given this, D-mannitol is extremely promising in the application to TES.

Currently, the low thermal conductivity of PCM is one of the leading problems for efficient energy harvesting. This limitation reduces the melting/solidification rate of PCM and has led efforts to increase the thermal conductivity. Researchers have come up with a number of effective methods, including microencapsulation [2-4], porous media composite PCMs [5-10], and the addition of high thermal conductivity nanoparticles [11-13]. Among them, the microcapsule is beneficial to prevent liquid leakage while slightly improving the thermal conductivity. For porous composite PCM, a higher effective thermal conductivity could be realized as well as shape stabilization during phase change. In detail, Nada et al. [14] studied the composite PCM of porous carbon foam with different porosities and different thermal conductivities as energy storage material. Karthik et al. [15] studied the heat transfer characteristics of paraffin-filled graphite foam. Compared with pure paraffin wax, the use of graphite foam resulted in an improvement by 11 times in thermal conductivity, reduced the charge and discharge time by 30 % and 66 %, respectively, and reduced the latent heat by 22 %. Wang et al. [16] proposed a gradient porous metal foam-enhanced heat transfer system. Their results indicated that the gradient pore copper foam significantly improved the heat transfer capacity of the PCM. Moreover, its inclusion improved the temperature uniformity of the heat storage unit, and shortened the melting time by 37.6 %. This research was the first time to confirm the utility of gradient porous metal foam in a heat transfer system, and that its application improved the performance of the energy storage system. Feng et al. [17] conducted melting and solidification experiments and simulations on paraffin/graphene aerogel composite materials, and proved that the small-scale pore size contributes to the uniform phase change of the melting process and the uniform heat transfer temperature distribution. Yang et al. [18] combined a multi-layer PCM with a gradient cell foam and established a multi-stage parallel foam model to study the effect of the solidification evolution of the composite PCM. At present, the research on porous foam has been mostly concentrated on those foams with uniform pore size and porosity, but few studies regarding the effect of changing the pore size and porosity in the same system. In addition, Hoseinzadeh et al. [19, 20] carried out some numerical investigations of the melting process of PCMs in porous media

and rectangular container based on the enthalpy model and Darcy's model. The analytical methods such as collocation method, homotopy perturbation method and homotopy analysis method can be used as references for similar researches in the future.

With regard to the addition of nanostructures into PCM, a nanostructure-enhanced nanophase and alter the inherent PCM material properties can be produced. Fig. 1 shows the classification of nanoparticles as PCM additives. Liu et al. [21] used a chemical reduction method to prepare nanofluids containing metallic copper particles. When the volume fraction of copper nanoparticles was 0.2 %, the thermal conductivity of the nanofluids gradually decreased with time and did not require the addition of any dispersants or surfactants. Past studies have also indicated that copper nanoparticles with high thermal conductivity and with the surface area of larger particles are the key to improving thermal conductivity. To this end, Neeraj Gupta et al. [22] dispersed metal (Fe, Cu) nanoparticles into inorganic salt hydrate magnesium sulfate hexahydrate at a mass fraction of 0.5 %. Metal oxide particles (e.g., CuO [23], $Al_2O_3$ [24, 25], $TiO_2$ [26], $Fe_3O_4$ [27]) have been studied regarding their thermal conductivity and heat transfer enhancement effects on nanofluids. Shi et al. [28] compared the improvement of thermal conductivity in PCM after addition of either xGnP or graphene. Nomura et al. [29] compared two methods for preparing PCM and carbon fiber composites and measured the effective thermal conductivity of the composite PCM using laser flash evaporation. Carbon nanotubes are also an excellent carbon-based additive material. Moreover, carbon nanotubes with a relatively large length and diameter have higher axial thermal conductivity. For instance, Li et al. [30] prepared stearic acid/multi-walled carbon nanotube composites. The addition of only 3 % mass fraction of multi-wall carbon nanotubes (MWCNTs) increased the thermal conductivity by 5.7 %. Other studies have focused on different allotropes of carbon, such as expanded graphite [31], spherical graphite [32], graphite powder [33], and graphene aerogel [34]. To effectively improve the dispersion effect of nanoparticles in PCM, Nourani et al. [35] used sodium stearoyl lactylate as a surfactant in combination with ultrasonic vibration. It can be seen that past studies have only used a single method to strengthen the thermal conductivity of the PCM and few studies have accounted for the joint strengthening effect of porous frameworks-nanoparticles on the heat storage performance.

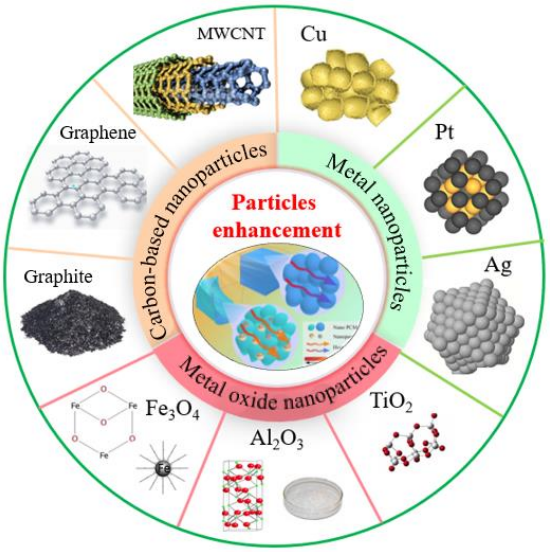


Fig. 1. Three main types of nanoparticles used as PCM additives.

In this paper, based on the concept of bionics, a vertical-horizontal dual-gradient-porous ceramic framework is innovatively proposed for reference to natural biological stem structure and animal tibia structure. Investigate the superiority of the new frame structure design in heat storage and transfer performance. On this basis, we adopted a dual strengthening method to build a framework-PCM-nanoparticle composite.

Existing studies have paid more attention to the multi-empty framework structure with uniform pore size or single gradient (vertical or horizontal). We proposed the vertical-horizontal double gradient aperture structure to improve phase change performance for the first time. Here, the PCM was combined with the vertical-horizontal double gradient pores. Subsequently, high thermal conductivity nanoparticles were added to improve the effective thermal conductivity of the composite material. The types of nanoparticles include graphite and carbon fiber particles. Predictions regarding the heat storage density, effective thermal conductivity, and overall melting time of the composite material indicated what nanoparticle additive was the best. Finally, we compared the improvement on the effective thermal conductivity and phase interface evolution using different addition amounts (2 %, 5 %, 7 %, 10 %) of the selected nanoparticle.

# 2. Simulation

## 2.1 Physical model

A porous framework structure model is constructed based on the gradient pore structure of organisms in nature. As shown in Fig. 2, the cell pores of plant stems grow from small to large from outside to inside. The small external pores result in a high strength due to the large proportion of the framework. To make sure the plants resist damage from external forces such as strong winds during the growth process. The larger internal aperture can transport more water and nutrients. The

structure of the animal's tibia is similar. The external framework has a larger proportion and small gaps, ensuring the strength and rigidity of the bones, and playing a role of support and protection. The large internal gaps store more bone marrow. Imitating the changes in the structure of plant stems, construct a framework structure with pore diameter changes in the vertical direction. Animal tibia structure has small pores in the outer layer and large pores in the inner layer to build a framework structure with horizontal pore diameter changes, imitating the structural changes.

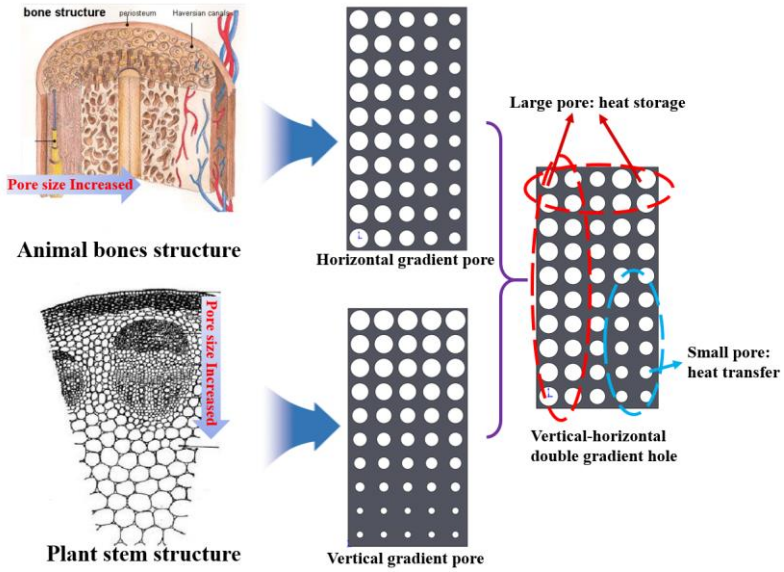


Fig. 2. The idea of constructing a gradient pore framework based on the concept of bionics.

We use the hexahedral unit center cutting sphere method to construct the unit framework. This was followed by Solidworks to perform Boolean operations on the hexahedron to obtain the framework model unit structure. As shown in Fig. 3, the unit side length was 100 μm, and the sphere radius ranged from 52 μm to 66 μm. The porous framework model had the following characteristics: (1) Simple geometric structure, thereby avoiding a large amount of calculations. (2) Important characteristics of real porous media were captured, along with the effects of relatively real reactions on the phase change process. (3) Changing the radius of the inscribed sphere allowed us to control the porosity changes and to construct a variety of arrangement models.

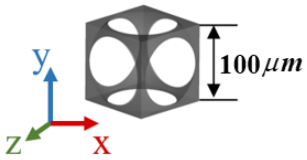


Fig. 3. Porous framework unit model.

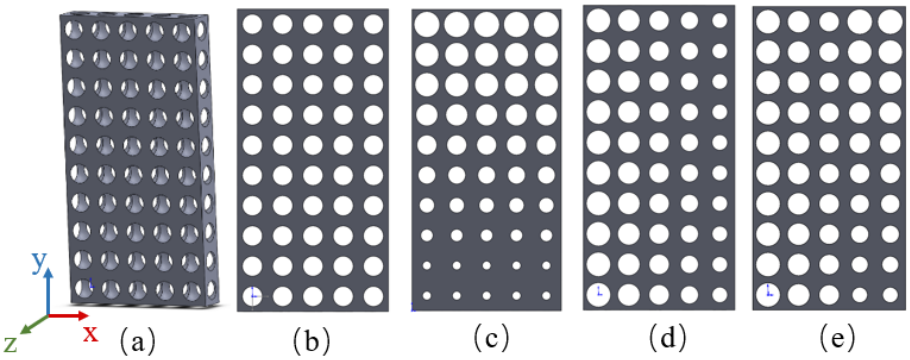


Fig. 4. Three-dimensional schematic diagram of model structure and front view of different structures: (a) three-dimensional structure diagram. (b) uniform pore structure. (c) vertical gradient pore structure. (d) horizontal gradient pore structure. (e) vertical-horizontal double gradient aperture structure.

We then assembled the unit model into a porous media model. The porous media structure was composed of 5 and 10 model units in the *x* and *y* directions, respectively, and 1 unit in the *z* direction. According to the pore size of the unit models, four framework structure models were then constructed. Fig. 4 shows the three-dimensional structure diagram of the composite unit and the front view of the four different framework structures (i.e., uniform pore structure, vertical gradient pore structure, horizontal gradient pore structure and vertical-horizontal double gradient pore structure). Of these, pore sizes were as follows: Uniform pore structure (120 μm diameter), vertical gradient pore structure (pore diameter change rate of 4 μm in the *y* direction), horizontal gradient pore structure (pore diameter change rate of 4 μm in the *x* direction), and vertical-horizontal double gradient pore structure (pore diameter change rate of 2 μm in the *x* direction and 2 μm in the *y* direction).

The initial temperature field of the composite material was set to an ambient temperature of 293 K. Since the initial state liquid phase rate was 0, all were solid PCMs and the initial velocity field was 0 in the three axes' directions. We considered the effect of gravity in this study, so the direction of gravity was 9.8 $m \cdot s^2$ in the negative direction along the y-coordinate axis.

We first initialized the overall temperature of the composite material and set the boundary temperature. The temperature of the entire composite material is a constant in the initial stage:

$$T(x,y,z,t)\big|_{t=0} = T_1 \tag{1}$$

Where $T_1$ is the initial temperature set during melting and $T_1$=293 K during melting.

The left boundary condition is set as:

$$T(x,y,z,t)\big|_{x=0} = 673K \tag{2}$$

The right boundary, top and bottom boundaries, and front and back boundaries conditions of the calculation domain are set to:

$$\left.\frac{\partial T(x,y,z,t)}{\partial x}\right|_{x=0.5}=0 \tag{3}$$

$$\left.\frac{\partial T(x,y,z,t)}{\partial x}\right|_{y=0,y=1}=0 \tag{4}$$

$$\left.\frac{\partial T(x,y,z,t)}{\partial x}\right|_{z=-0.1,z=0.1}=0 \tag{5}$$

To set the boundary conditions of the composite structure and to shorten the melting time, the boundary temperature was set higher. One side was a high-temperature heat source. The remaining boundaries were adiabatic boundaries. The calculation domain and boundary conditions are shown in Fig. 5:

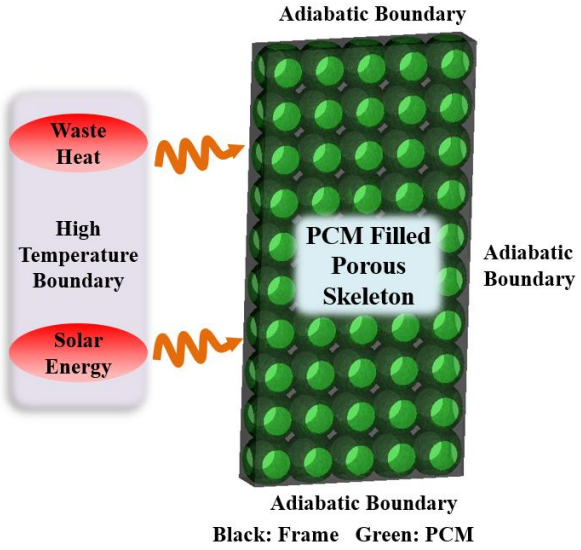


Fig. 5. Calculation area and boundary conditions

## 2.2 Mathematical model

The nonlinear characteristics of the solid-liquid phase change heat transfer process and the complexity of the porous framework structure make the coupling process of flow and heat transfer more complicated. To establish the mathematical model for this problem, the following assumptions were made:

(1) The liquid phase after melting of the PCM is an incompressible Newtonian fluid.

(2) Considering the natural convection in the liquid phase, the Boussinesq assumption is approximately applicable.

(3) In the process of phase transition, consider the existence of the mushy zone.

(4) Ignore radiation and assume the solid-liquid physical properties are constant.

(5) The porous framework material is rigid, uniform, isotropic, and full of PCMs.

Based on the above assumptions, the control equation of the three-dimensional numerical model of the PCM framework composite material can be expressed as:

Continuity equation:

$$\frac{\partial \rho}{\partial t} + \nabla \cdot (\rho \vec{u}) = 0 \tag{6}$$

Momentum equation of molten PCM [36,37]:

$$\rho \frac{\partial \vec{u}}{\partial t} + \rho (\vec{u} \cdot \nabla) \vec{u} = \nabla \cdot [-p\vec{I} + \mu(\nabla \vec{u} + (\nabla \vec{u})^T - \mu(\nabla \cdot \vec{u}))] + \vec{F} \tag{7}$$

Where $\vec{\mathrm{I}}$ is the vector sum of the *x*, *y*, and *z* directions. Gravity is considered in this problem. Therefore, the source term of the force $\vec{F}$ is defined in the momentum equation, which is composed of volume force $\vec{F}_V$ and thermal buoyancy $\vec{G}$. The volume force $\vec{F}_V$ is for molten PCM. These are denoted as:

$$\vec{F} = \vec{F}_V + \vec{G} \tag{8}$$

$$\vec{F}_V = -\frac{(1-\theta)^2}{\theta^3 + \lambda} A_{mush} \cdot \vec{u} \tag{9}$$

$$\vec{G} = \rho \beta \vec{g} (\mathrm{T} - \mathrm{T}_m) \tag{10}$$

Where $\vec{g}$ is the acceleration of gravity, $\beta$ is the coefficient of thermal expansion, $\mathrm{T}_m$ is the melting temperature of the PCM, and $A_{mush}$ is the mushy zone constant which will affect the transition of the phase interface.

Energy equation [33,34]:

$$\rho_g C_{P,\mathrm{g}} \frac{\partial T_g}{\partial t} + \rho_l C_P \frac{\partial T_l}{\partial t} = \nabla \cdot (\mathrm{k}_g \nabla \mathrm{T}_g + \mathrm{k}_e \nabla \mathrm{T}_l) + \dot{q} \tag{11}$$

Where $\dot{q}$ is the heat flux density of the heat source, $\rho_g$, $\mathrm{k}_g$, $C_{P,\mathrm{g}}$ are the density of the framework material, thermal conductivity and, specific heat capacity, $\mathrm{k}_e$ and $C_P$ are the equivalent thermal conductivity and equivalent specific heat capacity of the PCM, respectively, which are defined as[36,38]:

$$\mathrm{k}_e = \varepsilon \cdot k_l + (1-\varepsilon)\,\mathrm{k}_s \tag{12}$$

$$C_P = \begin{cases} C_{P,s} & \mathrm{T} \le \mathrm{T}_m \\ C_P + \dfrac{L}{\Delta T} & \mathrm{T}_m \le \mathrm{T} \le \mathrm{T}_m + \Delta T \\ C_{P,l} & \mathrm{T} \ge \mathrm{T}_m + \Delta T \end{cases} \tag{13}$$

The subscripts $s$ and $l$ represent solid and liquid parameters of the PCM, respectively. L is the latent heat of fusion, $\Delta T$ is the temperature range of the mushy zone, $\varepsilon$ is the liquid fraction, and the equation of the phase transition process is:

$$k_s \nabla T - k_l \nabla T_l = \theta \rho L \tag{14}$$

Convection heat transfer equation of molten PCM:

$$\rho C_P \frac{\partial T}{\partial t} + \rho C_P \vec{u} \cdot \nabla T = \nabla \cdot (\mathrm{k} \nabla \mathrm{T}) \tag{15}$$

In addition, we considered adding nanoparticles to PCM. According to both mass balance and mixing theories, the effective density of nano-PCM can be expressed as:

$$\rho_{nf} = \phi \rho_n + (1-\phi)\rho \tag{16}$$

According to the heat balance between nanoparticles and PCM, the effective heat capacity calculation formula proposed by Xuan and Roetzel [39] produces the effective specific heat capacity of nano-PCM:

$$(\rho C)_{nf} = \phi (\rho C_p)_n + (1-\phi)\rho C_p \tag{17}$$

The Boussinesq and latent heat terms of nano-PCM are calculated by the following formulae [40]:

$$(\rho \beta)_{nf} = \phi (\rho \beta)_n + (1-\phi)\rho \beta \tag{18}$$

$$(\rho \Delta H)_{nf} = (1-\phi)\rho \Delta H \tag{19}$$

Assuming that the nanoparticles are uniform, spherical particles that are uniformly dispersed in the PCM, the dynamic viscosity and effective thermal conductivity of the nano-PCM are given by the Brinkman relationship [41] and Maxwell model [42]:

$$\mu_{nf} = \frac{\mu}{(1-\phi)^{2.5}} \tag{20}$$

$$k_{nf} = \frac{k_n + 2k_e - 2(\mathrm{k}_e - \mathrm{k}_n)\phi}{k_n + 2k_e + 2(\mathrm{k}_e - \mathrm{k}_n)\phi} k_e \tag{21}$$

Where $\phi$ is the nanoparticle volume fraction, and the subscript $nf$ represents nano-PCM.

## 2.3 Material parameters and initialization

**Table 1.** Physical parameters of D-mannitol and calcium oxide ceramics

| Physical parameters | D-Mannitol (PCM) | Calcium oxide ceramics (framework) | Nano particles (graphite) | Nano particles (carbon fiber) |
|---|---|---|---|---|
| Density $\rho/\ \mathrm{kg\cdot m^{-3}}$ | 1520 | 2200 | 2090 | 1500 |
| Specific heat capacity $C_p/\ \mathrm{J\cdot kg^{-1}\cdot K^{-1}}$ | 2580 | 966 | 710 | 900 |
| Thermal conductivity $\lambda/\ \mathrm{W\cdot m^{-1}\cdot K^{-1}}$ | 1.32 | 15 | 200 | 700 |
| Latent heat $h/\ \mathrm{kJ\cdot kg^{-1}}$ | 316 | / | / | / |
| Thermal expansion coefficient | 3.085e-4 | / | / | / |
| Viscosity $\mu/\ \mathrm{kg\cdot m\cdot s^{-1}}$ | 4.65e-6 | / | / | / |

The physical properties of D-mannitol and calcium oxide ceramics used in the numerical simulation are shown in Table 1. The phase transition temperature of D-mannitol was not a fixed value, but a phase transition range. The solid phase temperature (i.e., temperature at which D-mannitol begins melting) and the liquid phase temperature (i.e., temperature at which D-mannitol begins solidifying) were 437 K and 440 K, respectively. The solid-phase and liquid-phase thermal conductivities were 1.32 $\mathrm{W\cdot m^{-1}\cdot K^{-1}}$ and 1.3 $\mathrm{W\cdot m^{-1}\cdot K^{-1}}$, respectively. The framework material was calcium oxide ceramics.

The unsteady solver based on the finite volume method in ANSYS Fluent was used to solve equations (6), (7), and (11), as well as the boundary and initial conditions. The momentum and energy control equations were discretized by the second-order upwind style. The pressure was discretized by the standard format. This is a recommended method for calculating natural convection. The pressure-velocity coupling adopted the SIMPLE algorithm. The temperature of the high-temperature heat source on the left was 673 K. To shorten the calculation time, the remaining

boundaries were set as adiabatic conditions.

# 3. Results and discussion

## 3.1 Porous material composite PCM

Under the condition that the left boundary temperature is 673 K, the other boundaries are adiabatic conditions. Fig. 6 shows the comparison of the melting process of uniform pore structure composite PCM relative to non-composite PCM. As indicated, the complete melting time for the uniform pore structure composite PCM was 247.5 ms. Comparatively, non-composite PCM was completely melted until 438.5 ms). The melting process was divided into three stages. Fig. 7 shows the change of the velocity field with time during the melting process of the homogeneous pore structure composite PCM. As shown, the first stage was the heat conduction stage. Since the PCM had just begun to melt, the flow velocity of the molten PCM was relatively low, and the convection effect was not obvious. Simultaneous to this, heat transfer was dominated by the heat conduction between the framework and the PCM, resulting in a faster melting speed. At this stage and since the convection effect was not obvious, the phase interface moved uniformly without tilting. Fig. 8 shows the change of the phase interface during the melting of the homogeneous pore structure composite PCM. Over time, the melting process entered the convection phase. At this stage, the overall temperature of the composite material gradually increased. As more and more PCM melted, the convection effect gradually increased. The fluid near the high temperature wall carried heat to the top of the composite material, where it released the heat. After the temperature decreased, the fluid flowed to the bottom. This pattern meant that the melting rate of the PCM at the top was higher than that at the bottom, resulting in an inclined phase interface. Due to the uneven temperature transfer along with the lower heat transfer effect of convection relative to that of the heat transfer effect, the overall melting rate of the composite material was reduced at this stage. Finally, the final stage of melting occurred. Due to the influence of natural convection, the solid-liquid interface was greatly tilted, resulting in uneven heat transfer of the composite material. In short, the temperature at the top was high, while that at the bottom temperature was low. this ultimately formed a triangular area in the lower right corner that did not easily melt, resulting in a melting rate that was further reduced. As shown in Fig. 6, the lower slope of the liquid phase rate curve in the final stage of melting indicated that the composite material melted more slowly in the final stage of melting. Integrating the analysis of these three stages and comparing with pure PCM, the introduction of the porous framework helps to improve the melting rate as a whole, which can accelerate the heat storage rate.

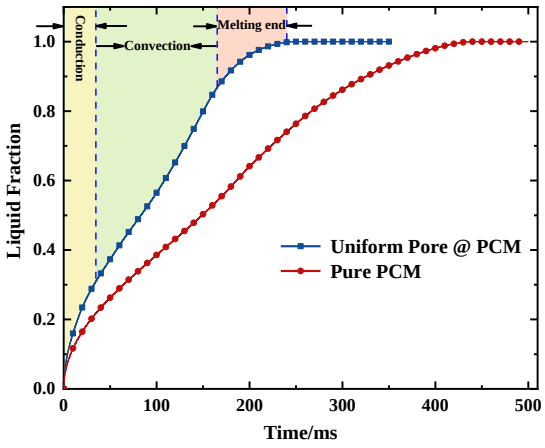


Fig. 6. Melting process of the uniform pore structure composite PCM and non-composite PCM.

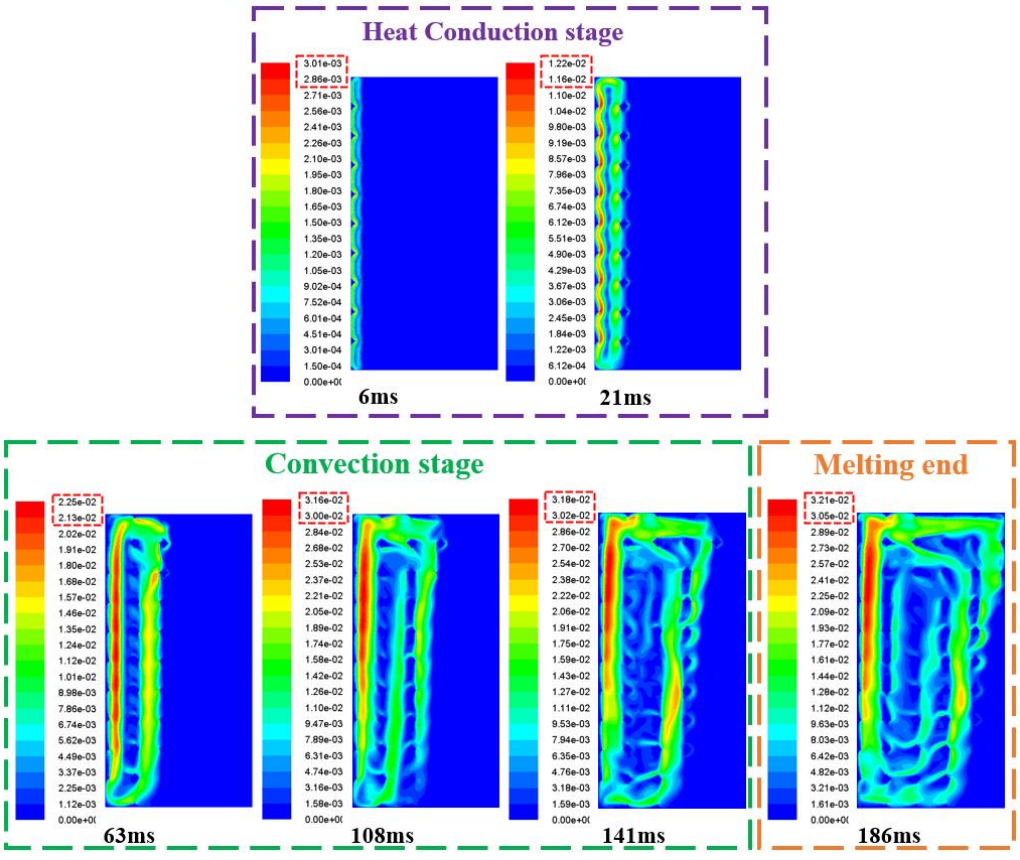


Fig. 7. Velocity field during the melting of a composite PCM with uniform pore structure.

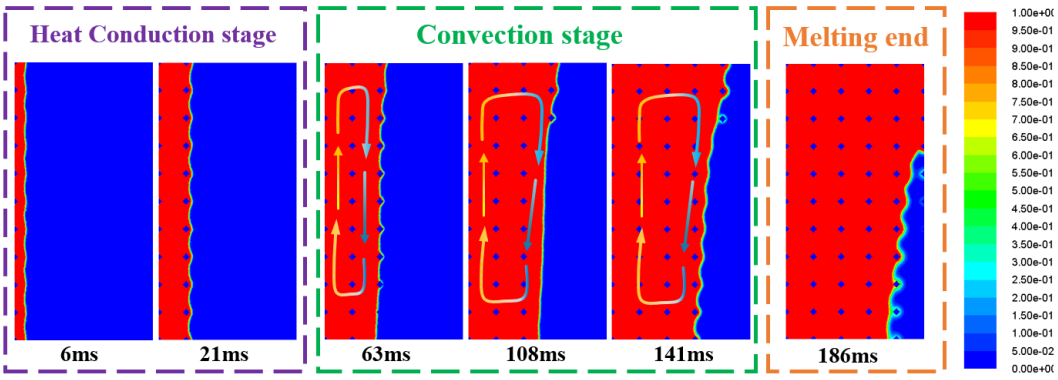

Fig. 8. Changes of phase interface during melting of composite PCM with uniform pore structure.

In view of the three stages of the melting process for the framework structure with uniform pore size framework structure—heat conduction, convection, and end of melting phases—we proposed the following heat transfer enhancement schemes: For the heat conduction zone, heat conduction was the main melting rate and should increase the porosity to ensure greater energy storage space. In the convection stage, the natural convection in the upper and lower regions was suppressed as much as possible to reduce the degree of inclination of the phase interface. Given this, the plan was to reduce the bottom pore diameter, such that flow possible occurred in the bottom pore and the local convection heat transfer in the bottom pore was strengthened. Convection in the upper and lower regions as well as the flow effect diagrams in the large and small pore are shown in Fig. 9. For the triangular region where the melting slows at the end of melting, we increased the framework proportion and used the heat conduction of the framework to strengthen the heat transfer process at this stage. Therefore, the vertical-horizontal double gradient pore structure proposed in this paper served as the framework to enhance the heat transfer effect of the composite material.

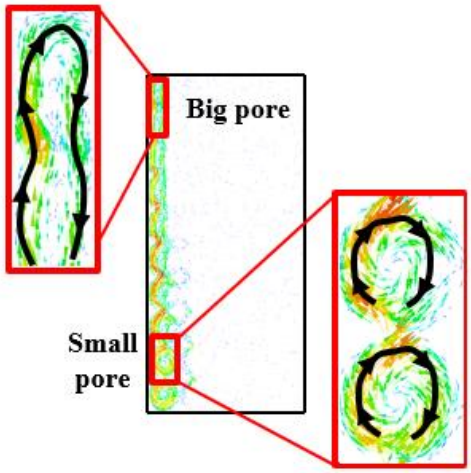


Fig. 9. Flow status across different pore sizes.

In this section, we propose (1) a vertical-horizontal double gradient pore structure, (2) increase in the pore size on the high-temperature wall, and (3) reduce the pore size at the bottom of the triangular area that is not easily melted. These changes were raised so that the heat transfer was properly conducted. In short, we propose solutions to enhance heat transfer in areas and stages where the melting rate is slower to promote the overall melting rate.

The uniform pore structure is also the most studied pore size distribution structure. At least some recent work has investigated the gradient change of the pore structure as a means to improve the framework structure's influence on heat transfer performance. Given this, there are both horizontal and vertical gradient aperture structures. Based on past research, we constructed a vertical-horizontal double gradient aperture framework structure and explored the overall melting

time of the composite material, movement of the phase interface, and improvements in its effective thermal conductivity. Past work has confirmed the superiority of the dual gradient aperture structure in enhancing heat transfer of PCMs.

Here, Fig. 10 compares the uniform pore size structure, vertical gradient change pore structure, horizontal gradient change pore structure, and vertical-horizontal double gradient change pore structure composite PCM in the melting process liquid fraction. Fig. 11 shows the change of the melting rate of the four structural composite PCMs across time. As shown, the highest melting rate occurred when the composite material melted in the initial stage. As indicated in Figs. 10 and 11 and when comparing to structures with vertical gradient, horizontal gradient, and uniform pore sizes, the double gradient pore size structure proposed here did not significantly reduce the melting rate at the end of melting. Moreover, the overall melting time of the composite material was 170 ms. Compared with the other three framework structures, this melting time was significantly shortened, and the heat storage efficiency was also improved.

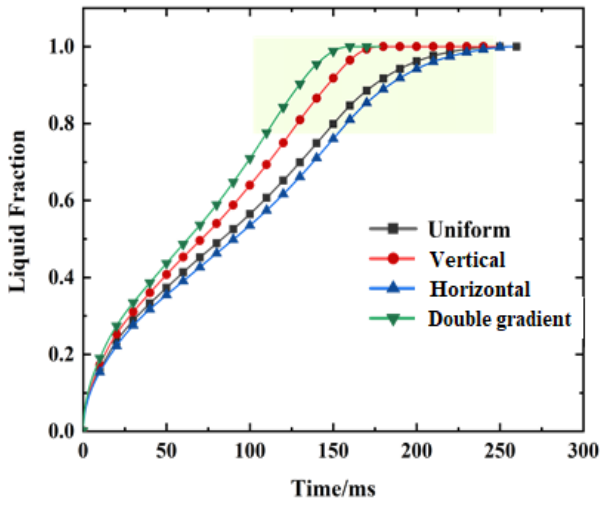


Fig. 10. Change of liquid phase rate of composite PCM with different framework structures across time.

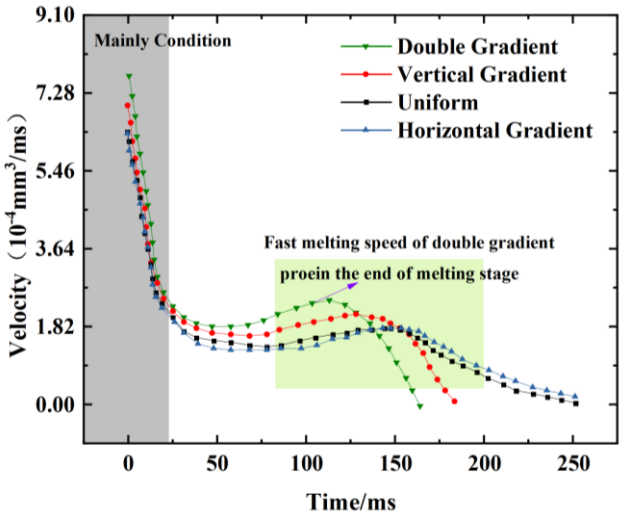


Fig. 11. Melting rate of different framework structure melting processes.

Fig. 12 compares the evolution of the phase interface at different moments of melting for non-composite PCM, homogeneous framework structure composite PCM, and vertical-horizontal double gradient pore composite PCM. As shown, the phase interface of the dual-gradient pore structure did not obviously tilt, which was beneficial to shortening the overall melting time and allowing for a more uniform, overall temperature of the composite material.

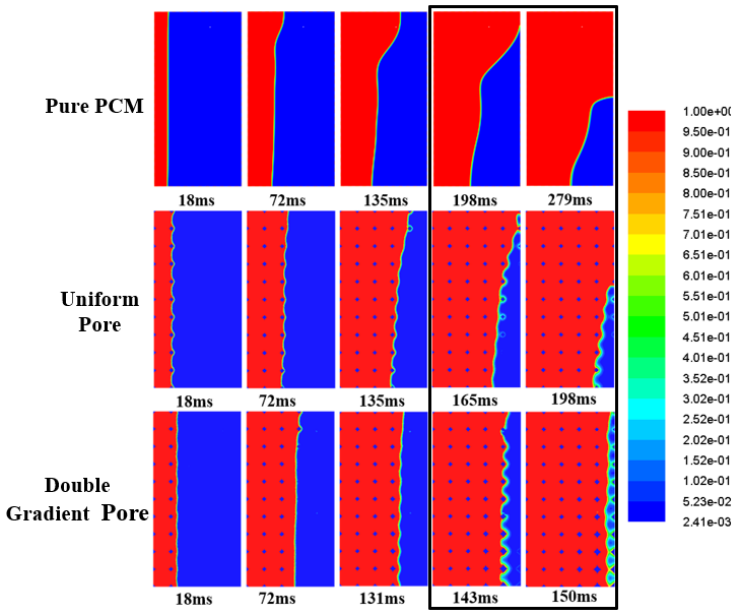


Fig. 12. Change of solid-liquid interface across time.

Fig. 13 shows the effect of improving the effective thermal conductivity during the melting process after compounding PCM with different framework structures. The thermal conductivity of the D-mannitol material used in this study was 1.32 $W \cdot m^{-1} \cdot K^{-1}$. As shown in Fig. 13, the vertical-horizontal double-gradient pore structure in the composite material had an effective thermal conductivity of 4.3 $W \cdot m^{-1} \cdot K^{-1}$, which was 226 % higher than that of non-composite PCM. Notably, this improvement was the best that achieved in this study and indicated a high thermal conductivity ceramic material. However, the optimized design of the framework structure also improved the effective heat transfer effect.

In addition, and under the premise of ensuring high thermal conductivity, the heat storage density of the composite material was studied. Fig. 14 shows a comprehensive comparison of the heat storage density and thermal conductivity of different frame structures. The heat storage density of the composite material included the sensible heats of both the framework and the PCM as well as the latent heat storage heat of the PCM. Results indicated that the heat storage was much larger than the sensible heat storage. The heat storage density also varied as there were slight differences in the porosity of different framework structures. However, the double gradient pore structure shown in

Fig. 14 stored heat while ensuring higher thermal conductivity. The heat storage density was also relatively high, which achieved the desired effect.

Therefore, in the design of the matrix framework, the dual gradient pore structure was determined to be superior to that of the uniform, horizontal, or vertical single gradient pore structures in terms of overall melting time, improvement of effective thermal conductivity, and phase interface transition.

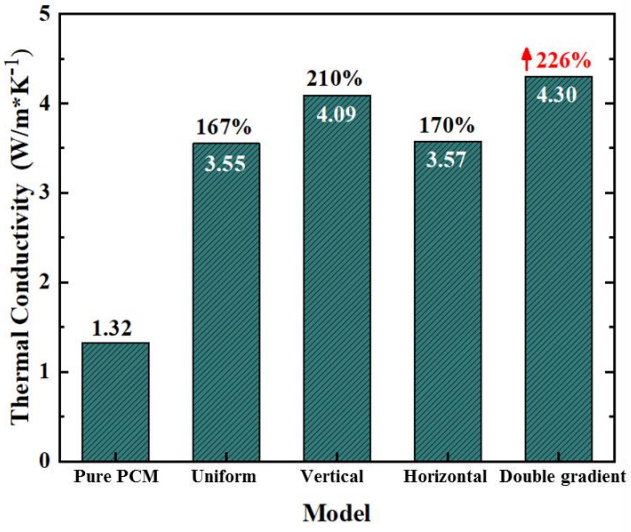


Fig. 13. Improvement of thermal conductivity for different framework structures.

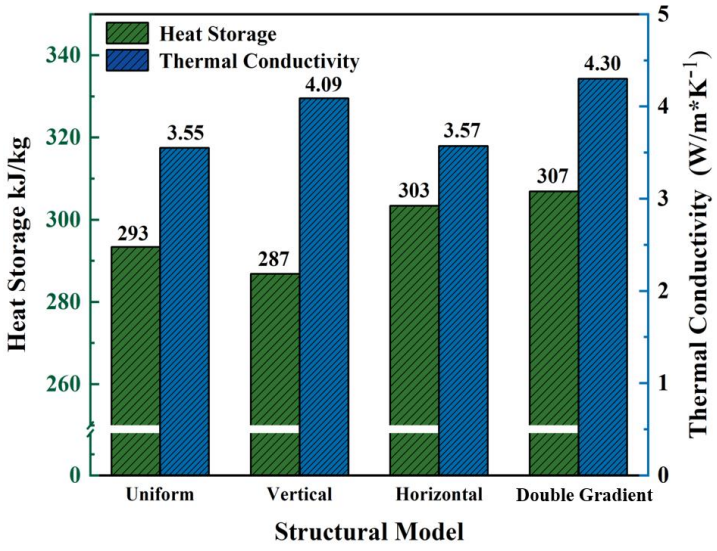


Fig. 14. Comprehensive comparison of heat storage density and improvement in thermal conductivity for different framework structures.

## 3.2 Nanoparticles added to PCM

To further improve the thermal conductivity of the composite material and construct a composite structure of framework-PCM-high thermal conductivity particles, we next used sheet graphite and columnar carbon fibers as thermal conductivity enhancers that were uniformly filled in the PCM. This approach adopted a single-phase model that ignored the interactions between

particles as well as the clusters effect. The effect of filling the PCM with 5 % volume fraction of lamellar graphite and columnar carbon fiber in the double gradient pore size framework structure on the overall thermal conductivity is shown in Fig. 15. These results showed that the addition of the two thermal conductivity enhancers improved overall thermal conductivity. Moreover, graphite addition had a better effect on the thermal conductivity of the composite material than that of the same volume fraction of carbon fiber. Although the intrinsic thermal conductivity of carbon fiber particles is higher than that of graphite particles, this is mainly because graphite is added as lamellar particles, and carbon fibers are columnar particles. The shape structure has a better effect on improving the effective thermal conductivity of PCMs.

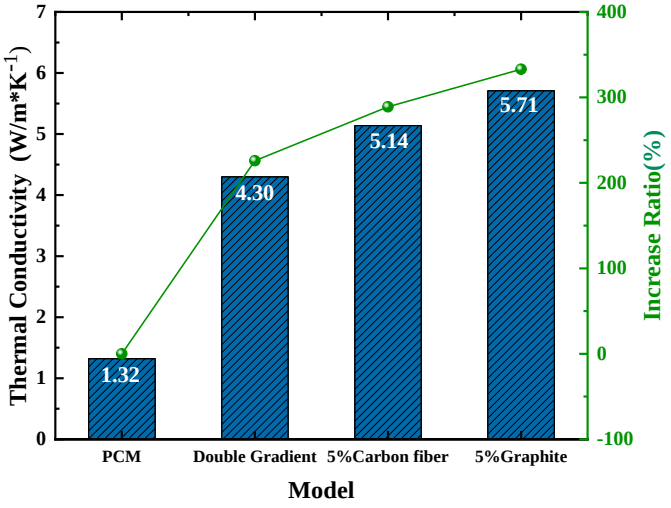


Fig. 15. Effect of nanoparticles on improving the effective thermal conductivity.

After adding nanoparticles to the framework-PCM composite material, the effective thermal conductivity increased and the melting time decreased. As the volume fraction of the PCM decreased, the heat storage density also decreased. To more fully reflect the heat storage performance after adding nanoparticles, we next introduced the concept of heat storage rate to comprehensively consider the overall melting time and heat storage. The heat storage rate was defined as the amount of heat absorbed by the composite PCM per unit mass from the initial temperature (solid state) to the complete melting of the PCM for a given unit of time ($kW \cdot kg^{-1}$). Fig. 16 shows the heat storage density comparison of composite structure doped with nanoparticles, which includes the framework structure, PCM, sensible heat for the nanoparticles, and latent heat storage of PCMs. As indicated, as the nanoparticle amount increased, heat storage gradually decreased. However, as nanoparticles increased, the time required for complete melting decreased, and the heat was stored in a shorter amount of time. Fig. 17 compares the heat storage efficiency of composite materials with the addition of different nanoparticles.

After adding the nanoparticles, the heat storage efficiency gradually increased. Therefore, selecting the correct, corresponding heat-conducting particle to add to a specific heat storage system became necessary. For instance, energy power plants require high heat storage, but the requirements for heat storage time are not strict. Given this, they can absorb heat over a long period of time. Under these conditions, a smaller amount of nanoparticles would be needed. Comparatively, some industrial waste heat recovery systems have heat released over a short amount of time. Given this, the thermal response time of the heat storage system is required to be as short as possible. This part of the waste heat is absorbed and stored in the composite material over this short time period. Such systems would need to ensure heat storage and would require a larger amount of nanoparticles to improve response time and heat storage efficiency.

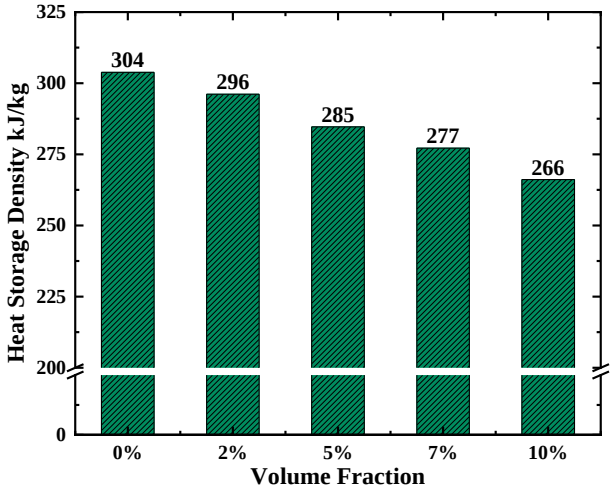


Fig. 16. Heat storage density of the composite structure doped with different nanoparticle amounts.

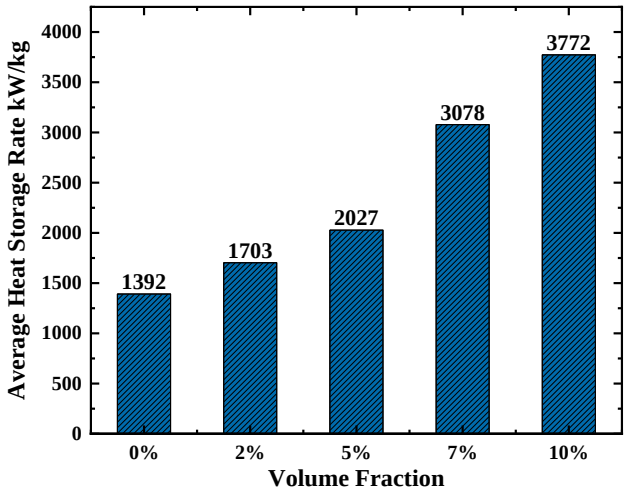


Fig. 17. Heat storage rate of composite structure doped with different nanoparticle amounts.

## 4. Conclusions

Inspired by the biological graded-pore structure, a vertical-horizontal double gradient pore framework was proposed to pack the medium PCM for the first time. The thermal storage properties

and heat transfer characteristics of the composites were explored, and the nanoparticles were added to get enhanced thermal conductivity. The main conclusions are as follows:

(1) The effective thermal conductivity of the vertical-horizontal dual gradient aperture ceramic filled with D-mannitol was 4.3 $W \cdot m^{-1} \cdot K^{-1}$, and enhanced 226 % from pure PCM. Compared with other framework structures, the reasonable design of the aperture structure that ensures a larger energy storage space and a more uniform solid-liquid interface movement, resulting in the significantly improved heat storage and heat transfer performance.

(2) Due to the introduction of the framework structure, the heat storage density was accordingly reduced. Nevertheless, compared with those frameworks with uniform pore distribution and single-gradient pore distribution, the heat storage density of the double-gradient pore structure remained as high as 307 $kJ \cdot kg^{-1}$ (97 % of pure PCM). That is, the composite material exhibits an improved the effective thermal conductivity as well as a higher heat storage density.

(3) Constructing a double-gradient pore framework-PCM-nanoparticle composite, the results showed that after adding 5 % carbon fiber and graphite, the thermal conductivity of the composite material reaches up to 5.14 $W \cdot m^{-1} \cdot K^{-1}$ and 5.71 $W \cdot m^{-1} \cdot K^{-1}$, respectively. It confirms that the double gradient pore framework-PCM-graphite particles serve together as the best counterpart.

Based on the research works mentioned above, it is believed that the bionic gradient pore structure has great potential in the development of heat storage PCM.

## Acknowledgement

The authors gratefully acknowledge the financial support from the National Key Research and Development Plan Project (No.2018YFA0702300), Beijing Natural Science Foundation (No.3192022) and the National Natural Science Foundation of China (No. 51876007).

## References

[1] D.L. Feng, Y.H. Feng, L. Qiu, P. Li，Y.Y. Zang，H.Y. Zou, Z.P. Yu，X.X. Zhang, Review on nanoporous composite phase change materials: Fabrication, characterization, enhancement and molecular simulation. Renewable and Sustainable Energy Reviews, 109 (2019) 578-605.

[2] J.J. Zhang, Z.G. Qu, Y. Liu, Numerical study on the melting thermal characteristics of a microencapsulated phase change plate, Numerical Heat Transfer, Part A: Applications 70 (4) (2016) 399-419.

[3] C. Mankel, A. Caggiano, N. Ukrainczyk, E. Koenders, Thermal energy storage characterization of cement-based systems containing microencapsulated-PCMs, Construction and Building Materials 199 (2019) 307-320.

[4] C.E. Li, H. Yu, Y. Song, H. Liang, X. Yan, Preparation and characterization of PMMA/TiO2 hybrid shell microencapsulated PCMs for thermal energy storage, Energy 167 (2019) 1031-1039.

[5] Z. Zhang, X. He, Three-dimensional numerical study on solid-liquid phase change within open-celled aluminum foam with porosity gradient, Applied Thermal Engineering 113 (2017) 298-308.

[6] C.Y. Zhao, W. Lu, Y. Tian, Heat transfer enhancement for thermal energy storage using metal foams embedded within phase change materials (PCMs), Solar energy 84 (8) (2010) 1402-1412.
[7] Y.Q. Zhao, L. Jin, B.Y. Zou, G. Qiao, T.T. Zhang, L. Cong, F. Jiang, C. Li, Y. Huang, Y.L. Ding, Expanded graphite–paraffin composite phase change material: effect of particle size on the composite structure and properties, Applied Thermal Engineering 171 (2020) 115015.
[8] Cai W, He F, Zhang Q, et al. Experimental and numerical simulation of phase change process for paraffin/expanded graphite/ethylene-vinyl acetate ternary composite[J]. Applied Thermal Engineering, 2020, 169: 114896.
[9] Liu X, Yang W, Feng Z, et al. A numerical investigation of heat transfer process in paraffin/ethylene-vinyl acetate/graphene aerogel ternary composite[J]. Applied Thermal Engineering, 2021, 190: 116800.
[10] Feng Z, Yang W, Liu X, et al. Experimental and numerical investigation of phase change progress for paraffin in hybrid aerogel of graphene and carbon nanotubes[J]. Applied Thermal Engineering, 2020, 178: 115633.
[11] S.A.M. Mehryan, M. Vaezi, M. Sheremet, M. Ghalambaz, Melting heat transfer of power-law non-Newtonian phase change nano-enhanced n-octadecane-mesoporous silica (MPSiO2), International Journal of Heat and Mass Transfer 151 (2020) 119385.
[12] F. Iachachene, Z. Haddad, H.F. Oztop, E. Abu-Nada, Melting of phase change materials in a trapezoidal cavity: Orientation and nanoparticles effects, Journal of Molecular Liquids 292 (2019) 110592.
[13] S.H. Tasnim, R. Hossain, S. Mahmud, A. Dutta, Convection effect on the melting process of nano-PCM inside porous enclosure, International Journal of Heat and Mass Transfer 85 (2015) 206-220.
[14] S.A. Nada, W.G. Alshaer, Comprehensive parametric study of using carbon foam structures saturated with PCMs in thermal management of electronic systems, Energy Conversion and Management 105 (2015) 93-102.
[15] M. Karthik, A. Faik, B. D'Aguanno, Graphite foam as interpenetrating matrices for phase change paraffin wax: A candidate composite for low temperature thermal energy storage, Solar Energy Materials and Solar Cells 172 (2017) 324-334.
[16] Z.F. Wang, J.N. Wu, D.Q. Lei, H. Liu, J.P. Li, Z.Y. Wu, Experimental study on latent thermal energy storage system with gradient porosity copper foam for mid-temperature solar energy application, Applied Energy 261 (2020) 114472.
[17] Z.C. Feng, Y.S. Li, F.F. He,Y.T. Li, Y.L. Zhou, Z.J. Yang, R. He, K. Zhang, W.B.Yang, Experimental and numerical simulation of phase change process for paraffin in three-dimensional graphene aerogel, Applied Thermal Engineering 167 (2020) 114773.
[18] X.H. Yang, W.B. Wang, C. Yang, L.W. Jin, T.J. Lu, Solidification of fluid saturated in open-cell metallic foams with graded morphologies, International Journal of Heat and Mass Transfer 98 (2016) 60-69.
[19] S. Hoseinzadeh, P. S. Heyns, A.J. Chamkha, A. Shirkhani, Thermal analysis of porous fins enclosure with the comparison of analytical and numerical methods, Journal of Thermal Analysis and Calorimetry 138 (2019) 727 – 735.
[20] S. Hoseinzadeh, R. Ghasemiasl, A.J. Chamkha, Numerical investigation of rectangular thermal energy storage units with multiple phase change materials, Journal of Molecular Liquids 271 (2018) 655-660.

[21] M.S. Liu, M.C.C. Lin, C.Y. Tsai, C.C. Wang, Enhancement of thermal conductivity with Cu for nanofluids using chemical reduction method, International Journal of Heat and Mass Transfer 49 (17-18) (2006) 3028-3033.

[22] N. Gupta, A. Kumar, S.K. Dhawan, H. Dhasmana, A. Kumar, V. Kumar, A. Verma, V.K. Jain, Metal nanoparticles enhanced thermophysical properties of phase change material for thermal energy storage, Materials Today: Proceedings 32 (2020) 463-467.

[23] M.H. Esfe, S. Saedodin, M. Akbari, A. Karimipour, M. Afrand, S. Wongwises, M.R. Safaei, M. Dahari. Experimental investigation and development of new correlations for thermal conductivity of CuO/EG–water nanofluid, International Communications in Heat and Mass Transfer 65 (2015) 47-51.

[24] S. Hoseinzadeh, S. Heyns, H. Kariman, Numerical investigation of heat transfer of laminar and turbulent pulsating Al2O3/water nanofluid flow, Energy conversion and management 30 (2019) 1149-1166.

[25] S. Hoseinzadeh, S. Heyns, R. Ghasemiasl, Experimental analysis to improving thermosyphon (TPCT) thermal efficiency using nanoparticles/based fluids (water), European Physical Journal Plus 132 (2017) 197.

[26] R.M. Mostafizur, M.H.U. Bhuiyan, R. Saidur, A.R. Abdul Aziz, Thermal conductivity variation for methanol based nanofluids, International Journal of Heat and Mass Transfer 76 (2014) 350-356.

[27] W. Yu, H.Q. Xie, L.F. Chen, Y. Li, Enhancement of thermal conductivity of kerosene-based Fe3O4 nanofluids prepared via phase-transfer method, Colloids and surfaces A: Physicochemical and engineering aspects 355 (1-3) (2010) 109-113.

[28] J.N. Shi, M.D. Ger, Y.M. Liu, Y.C. Fan, N.T. Wen, C.K. Lin, N.W. Pu, Improving the thermal conductivity and shape-stabilization of phase change materials using nanographite additives, Carbon 51 (2013) 365-372.

[29] T. Nomura, K. Tabuchi, C.Y. Zhu, N. Sheng, S.F. Wang, T. Akiyama, High thermal conductivity phase change composite with percolating carbon fiber network, Applied energy 154 (2015) 678-685.

[30] T.X. Li, J.H. Lee, R.Z. Wang, Y.T. Kang. Enhancement of heat transfer for thermal energy storage application using stearic acid nanocomposite with multi-walled carbon nanotubes, Energy 55 (2013) 752-761.

[31] Z.W. Huang, X.N. Gao, T. Xu, Y.T. Fang, Z.G. Zhang, Thermal property measurement and heat storage analysis of LiNO3/KCl–expanded graphite composite phase change material, Applied energy 115 (2014) 265-271.

[32] J. Lopez，G. Caceres，E.P.D. Barrio，W. Jomaa, Confined melting in deformable porous media: A first attempt to explain the graphite/salt composites behavior, International Journal of Heat and Mass Transfer 53 (5-6) (2010) 1195-1207.

[33] S. Azeem, M. Zain-ul-Abdein, Investigation of thermal conductivity enhancement in bakelite–graphite particulate filled polymeric composite, International Journal of Engineering Science 52 (2012) 30-40.

[34] Y.J. Zhong, M. Zhou, F.Q. Huang, T.Q. Lin, D.Y. Wan, Effect of graphene aerogel on thermal behavior of phase change materials for thermal management, Solar Energy Materials and Solar Cells 113 (2013) 195-200.

[35] M. Nourani, N. Hamdami, J. Keramat, A. Moheb, M. Shahedi, Thermal behavior of paraffin-nano-Al2O3 stabilized by sodium stearoyl lactylate as a stable phase change material with high thermal conductivity, Renewable energy 88 (2016) 474-482.

[36] S.S. Sundarram, W. Li, The effect of pore size and porosity on thermal management performance of phase change material infiltrated microcellular metal foams, Applied thermal engineering 64 (1-2) (2014)147-154.

[37] S.S. Feng, M. Shi, Y.F. Li, T.J. Lu, Pore-scale and volume-averaged numerical simulations of melting phase change heat transfer in finned metal foam, International Journal of Heat and Mass Transfer 90 (2015) 838-847.
[38] S. Krishnan, J.Y. Murthy, S.V. Garimella, A two-temperature model for solid-liquid phase change in metal foams, Journal of heat transfer 127 (9) (2005) 995-1004.
[39] Y.M. Xuan, W. Roetzel, Conceptions for heat transfer correlation of nanofluids, International Journal of heat and Mass transfer 43 (19) (2000) 3701-3707.
[40] J.M. Khodadadi, Y. Zhang, Effects of buoyancy-driven convection on melting within spherical containers, International Journal of heat and mass transfer 44 (8) (2001) 1605-1618.ff
[41] H.C. Brinkman, The viscosity of concentrated suspensions and solutions, The Journal of Chemical Physics 20 (4) (1952) 571-571.
[42] J.C. Maxwell, A Treatise on Electricity and Magnetism, 3rd edition. Dover, New York, 1954.